processes

MDPI

Article

Molecular Simulation of Ultra-Microstructural Characteristics of Adsorption Pores in Terms of Coal and Gas Adsorption Properties

Pan Chen [1,2], Yanping Wang [1], Yanxia Zhao [3,*], Qi Wang [1], Zhihui Wen [1,4,5] and Ligang Tang [6,*]

1 College of Safety Science & Engineering, Henan Polytechnic University, Jiaozuo 454000, China; jmchenpan@163.com (P.C.); wyp@home.hpu.edu.cn (Y.W.); w19513251633@163.com (Q.W.); wenzhihui@hpu.edu.cn (Z.W.)
2 JiaoZuo Coal Industry (Group) Co., Ltd., Jiaozuo 454150, China
3 School of Mathematics & Information Science, Henan Polytechnic University, Jiaozuo 454000, China
4 State Key Laboratory Cultivation Base for Gas Geology and Gas Control, Henan Polytechnic University, Jiaozuo 454000, China
5 State Collaborative Innovation Center of Coal Work Safety & Clean-Efficiency Utilization, Jiaozuo 454000, China
6 School of Mine Safety, North China Institute of Science & Technology, Sanhe 065201, China
* Correspondence: zhaoyanxia001@126.com (Y.Z.); laotangx@126.com (L.T.)

Abstract: To investigate the ultra-microstructural characteristics and adsorption properties of coal pores, the pore structure of Dongsheng lignite and Chengzhuang anthracite in Qinshui Basin was characterized by the liquid nitrogen adsorption method. It was found that the SSA of micropores constituted more than 65% of the total SSA in both coal samples. The macromolecular model of coal and the N_2 molecular probe were used to obtain the ultrastructure parameters, and the gas adsorption behaviors of the two coals under different conditions were simulated by Grand Canonical Monte Carlo (GCMC) and Molecular Dynamics (MD). The results show that the pores of the lignite are mainly small pores, while the pores of the anthracite are mainly micropores. The specific surface area of the adsorption pores mainly constitutes micropores and ultra-micropores. The adsorption capacity of the CH_4 of anthracite is consistently higher than that of lignite. The CH_4 adsorption amount is positively correlated with the specific surface area and pore volume. This indicates that the gas adsorption capacity of coal is concentrated in micropores and ultra-micropores. The adsorption capacity increases with the increase in pressure and decreases with the increase in temperature. In the competitive adsorption of $CH_4/CO_2/H_2O$, the adsorption quantity is in the order of $H_2O > CO_2 > CH_4$. The research results provide a theoretical basis for coalbed methane exploitation and methane replacement.

Keywords: coal pore structure; molecular probe; ultra-micropore; coal macromolecular model; gas adsorption

check for updates

Academic Editor: Raymond Cecil Everson

Received: 9 February 2025
Revised: 5 March 2025
Accepted: 6 March 2025
Published: 7 March 2025

Citation: Chen, P.; Wang, Y.; Zhao, Y.; Wang, Q.; Wen, Z.; Tang, L. Molecular Simulation of Ultra-Microstructural Characteristics of Adsorption Pores in Terms of Coal and Gas Adsorption Properties. *Processes* **2025**, *13*, 771. https://doi.org/10.3390/pr13030771

Copyright: © 2025 by the authors. Licensee MDPI, Basel, Switzerland. This article is an open access article distributed under the terms and conditions of the Creative Commons Attribution (CC BY) license (https://creativecommons.org/licenses/by/4.0/).

1. Introduction

The coal industry, as the cornerstone of industrialization, will continue to dominate global energy production and consumption for a long time in the future [1–3]. Coal is an organic, porous, and heterogeneous material characterized by a vast system of pores and fractures, which forms an interconnected network structure [4,5]. This structure not only provides ample space for gas adsorption but also serves as a channel for gas migration [6,7]. Research on the ultra-microstructural characteristics and adsorption properties of coal

pores holds significant theoretical importance for the development of coalbed methane and the methane displacement within coal seams.

As global research on coal pore structures deepens, more sophisticated testing methods have been applied to coal porosity measurements, each offering unique advantages in the structural characterization of pores. Common testing methods for studying pores in coal include scanning electron microscopy (SEM), nano-CT imaging, nuclear magnetic resonance (NMR), high-pressure mercury injection, low-temperature CO_2 adsorption, and low-temperature liquid N_2 adsorption [8–11]. The complexity of pore structures in coal can be quantitatively characterized based on pore volume (PV), specific surface area (SSA), porosity, pore shape factors, fractal geometry, and other features [12–14]. Liu et al. [15] used low-temperature liquid nitrogen adsorption to quantitatively characterize the microstructure and pore distribution of coal samples with different metamorphic degrees (anthracite, bituminous coal, and lignite). However, due to the inability of N_2 molecules to penetrate pores smaller than their own diameter, the low-temperature liquid nitrogen adsorption technique is limited to measuring only a fraction of micropores. Li et al. [16] employed a combination of high-pressure mercury injection, low-temperature CO_2 adsorption, and low-temperature liquid nitrogen adsorption to jointly characterize the full pore size range of four coal samples from the Lu'an mining area. Furthermore, Ren et al. [17] combined low-temperature CO_2 adsorption, low-temperature liquid N_2 adsorption, and NMR to systematically investigate the pore structure and fractal characterization of coal. Therefore, it is evident that the combination method for characterization serves as an effective means for comprehensively and quantitatively assessing pore characteristics.

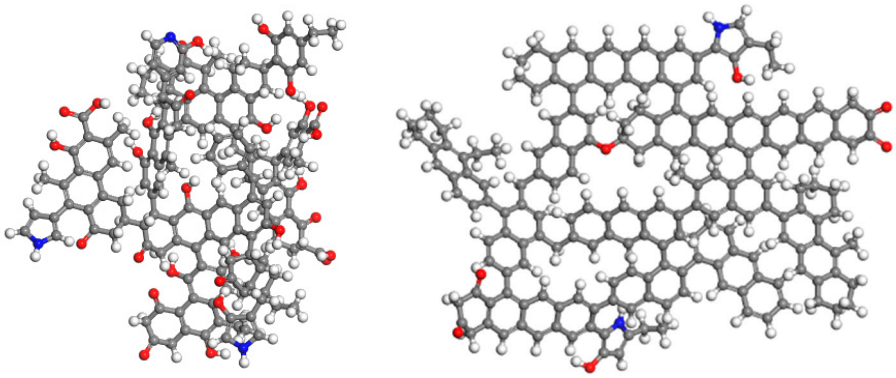
It has been reported that the micropores and ultra-micropores of coal play a crucial role in CH_4 adsorption [18,19], and that oxygen-containing functional groups play a secondary role in gas adsorption [20]. Ren et al. [21] have demonstrated that during the surface acidification modification of coal using Fenton reagents, a significant amount of oxygen-containing functional groups can be generated on the inner surface of coal. However, the isothermal adsorption capacity of coal under different concentrations showed little difference, indicating that the impact of oxygen-containing functional groups on coal adsorption was relatively minor. Han et al. [22] constructed a 4 nm pore structure as a methane migration channel and then analyzed the differences in the methane adsorption characteristics of coal with different metamorphic degrees, temperatures, and pressures. Wang et al. [23] found that the total PVs and SSAs of different-rank coal samples all exhibited a U-shaped variation pattern and analyzed the influence of pore structure on CH_4 adsorption capacity. Jiang et al. [24] investigated the impact of pore structure on gas adsorption in low-rank coal, revealing a positive correlation between Langmuir volume and both micropore PV and SSA. Specifically, a greater micropore PV and SSA corresponded to a stronger gas adsorption capacity. However, due to experimental limitations, it is challenging to measure ultra-micropores in coal. Some researchers have employed molecular modeling and simulation techniques to determine ultra-micropore structures. Wang [25] simulated and calculated the pore parameters of Dongqu No. 2 coal with the aid of Materials Studio and measured the pore parameters in the aggregated structure model by utilizing molecules with different radii as probes. Wang et al. [26] employed van der Waals force probes to visualize coal pore space and quantitatively analyze pore structure parameters. Yan et al. [27] utilized molecular simulation to study the influences of temperature, pressure, and moisture content on CO_2 and CH_4 adsorption in a macromolecular model of coal from Chicheng Mine, as well as the underlying microscopic mechanisms. Combining physical experiments with molecular simulation offers remarkable advantages in the ultra-microstructural characterization of adsorption pores.

This study selected two coal samples of different metamorphic degrees, i.e., Dongsheng lignite and Chengzhuang anthracite, as research objects. The comprehensive quantitative characterization of their adsorption pore structures was realized by low-temperature nitrogen adsorption experiments. Then, macromolecular models of lignite and anthracite were constructed using Grand Canonical Monte Carlo (GCMC) and Molecular Dynamics (MD) methods. Meanwhile, N_2 molecules were employed as probes to simulate and calculate the SSAs and PVs of the coal samples, and thus their ultra-micropore structural characteristics were obtained. Moreover, the adsorption properties of the lignite and anthracite macromolecular models were simulated under various pressures, temperatures, and adsorbates. This study is expected to elucidate the ultra-micropore structural characteristics and adsorption properties of coal, thereby establishing a foundational basis for further exploration of the interaction mechanisms between gas molecules and coal. Additionally, it offers theoretical support for coalbed methane extraction and methane displacement within coal seams.

2. Experimental and Simulation Methodology

2.1. Molecular Model Construction

Two coal samples with different metamorphic degrees, i.e., low-rank Dongsheng lignite (hereafter referred to as DS-L) and high-rank Chengzhuang anthracite (hereafter referred to as CZ-A), were selected for the experiment. A previous study by our research team [28] has offered a comprehensive explanation of the specific methods and processes used to construct the molecular structure model of CZ-A. Correspondingly, the molecular structure model of DS-L was constructed in the same manner. The final initial 3D macromolecular models of coal are displayed in Figure 1, and the detailed parameters are listed in Table 1.



(**a**) (**b**)

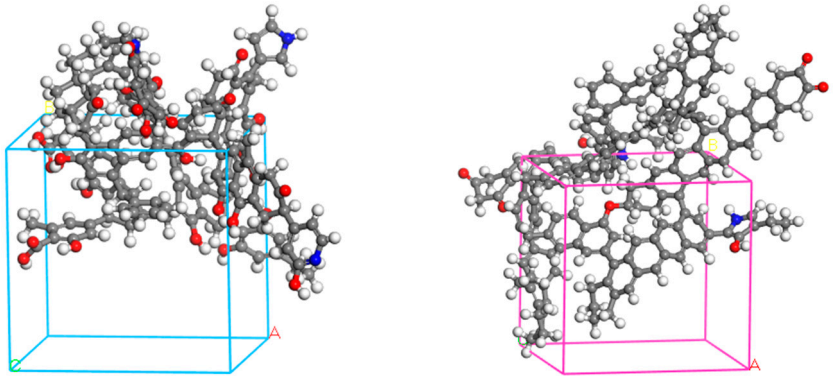
Figure 1. (**a**) Initial 3D molecular model of DS-L. (**b**) Initial 3D molecular model of CZ-A.

Table 1. Detailed parameters of the molecular model.

Coal Sample	Element Formula	Ultimate Analysis			
		C	H	O	N
DS-L	$C_{153}H_{139}N_3O_{29}$	73.99	5.64	18.68	1.69
CZ-A	$C_{188}H_{138}N_2O_7$	89.00	5.48	4.41	1.10

The constructed model structures were optimized through geometric refinement and annealing dynamics to obtain globally energy-optimized molecular models. Subsequently, periodic boundary conditions were applied to the optimized macromolecular models for density simulations. By continuously varying the model density, molecular potential energy

systems at different densities were obtained. The densities corresponding to the lowest energies in the DS-L and CZ-A molecular model systems were determined to be 1.30 g/cm^3 and 1.45 g/cm^3, respectively, representing the optimal densities for the molecular models. The corresponding periodic stable molecular models are depicted in Figure 2a,b.



(**a**) DS-L (**b**) CZ-A

Figure 2. (**a**) Macromolecular model of DS-L under periodic boundary conditions. (**b**) Macromolecular model of CZ-A under periodic boundary conditions.

2.2. Liquid Nitrogen Adsorption Experiment

The pore structure characteristics of the experimental coal samples were determined through the liquid nitrogen adsorption experiment. The particle sizes of the experimental coal samples ranged from 0.18 to 0.25 mm. The measured contents included the SSA, PV, and pore structure characteristics of the coal samples. The experiment employed the V-sorb2800 SSA and pore size analyzer produced by Beijing Jinaipu Company (Beijing, China), which featured a pore size measurement range of 0.35–500 nm and an SSA lower limit of 0.01 m^2/g. The static volumetric method was employed, utilizing liquid nitrogen with a purity of ≥99.999% as the adsorbate at −196 °C (77.15 K) during the adsorption process.

2.3. Simulation of Coal Pore Structure Characteristics

The SSAs and PVs of the DS-L and CZ-A macromolecular models were simulated with the aid of Materials Studio. In the simulation, the Atom Volumes & Surface module within the Tools toolbar was utilized, and the coal macromolecular models were calculated based on the Connolly principle. In addition, the Atom Volumes & Surfaces tool was selected, and then a Connolly Surface was established, with the Connolly radius set to 1.84 Å (equivalent diameter of a nitrogen molecule). The remaining parameters were left at their default settings.

2.4. Optimization of the Model

The parameters were set as follows: Geometry optimization: The energy standard deviation was 0.00002 Kcal/mol; the atomic root mean square was 0.001 Kcal/mol/Å; the maximum iteration step was 50,000; the force field was COMPASS; the charge was Charge using QEq; the Coulomb force and van der Waals force were both atom-based; and the accuracy was ultra-fine. Annealing optimization: The number of cycles was 10; the initial temperature was 300 K; the maximum temperature was 600 K; the amplitude of each heating or cooling was 5 K; the ensemble was NVT ensemble; the time was 1.0 fs; the temperature control method was nose; the force field was Dreiding; the charge was charge using QEq; the Coulomb force and van der Waals force were both atom-based; and the accuracy was ultra-fine.

2.5. Adsorption Simulation

The specific parameter settings for the simulation were as follows: The task was set to adsorption isotherm, and the Monte Carlo method and the Grand Canonical ensemble were adopted. The simulation temperature was set to 303.15 K (30 °C), and the pressure ranged from 0 kPa to 10,000 kPa, with the gradient being 1000 kPa. The fugacity steps were set to 10, the equilibration steps to 100,000 (which meant that the first 100,000 steps of the simulation were used to reach equilibrium), and the production steps to 1,000,000 (which meant that the subsequent 1,000,000 steps were used to collect statistics on the studied adsorption properties). In addition, the COMPASS force field and Charge using QEq were selected. Both the electrostatic and van der Waals forces were set to atom-based, and the simulation precision was set to fine.

3. Results and Discussion

3.1. Pore Structure Characteristics of Coal

(1) PV distribution characteristics

Aiming at exploring the pore size distribution of coal samples with varying metamorphic degrees, the data obtained from the liquid nitrogen adsorption experiments were analyzed with the aid of the inherent Barrett–Joyner–Halenda (BJH) theoretical model in the software. This model, rooted in the Kelvin equation, is a robust model for determining pore size distribution. Based on the principle of capillary condensation, it can be expressed by Equation (1):

$$r_k = -\frac{2\sigma_1 V_{\mathrm{ml}}}{RT_{\mathrm{b}} ln(P/P_0)} \quad (1)$$

where r_k is the pore radius of the experimental coal sample, nm; σ_1 is the surface tension of the condensed phase, N/M; V_{ml} is the adsorption volume of the liquid under the action of liquid nitrogen, cm^3/g; R is the gas constant, with a value of 8.314 $J \cdot mol^{-1} \cdot K^{-1}$; T_{b} is the experimental temperature, at 77 K in this study; P is the pressure of the adsorbate, Pa; and P_0 is the saturation vapor pressure of nitrogen at −196 °C, Pa.

To investigate the PV distribution characteristics of coal samples with varying metamorphic degrees, it is necessary to classify the pore diameters. To achieve this goal, the decimal classification standard proposed by B.B.Hodot was adopted; that is, pores in the coal samples were divided into micropores (<10 nm), small pores (10–100 nm), mesopores (100–1000 nm), and macropores (>1000 nm). The PV distribution results obtained from the experiments are illustrated in Table 2.

Table 2. PV test results of coal samples.

Coal Sample	BJH PV (mL/g)			Total PV (mL/g)
	Micropores	Small Pores	Mesopores	
DS-L	0.003318	0.006256	0.00288	0.012454
CZ-A	0.009209	0.005768	0.004665	0.019642

As can be observed from Table 2, the total PV of DS-L is 0.012454 mL/g, whereas that of CZ-A is 0.019642 mL/g. For DS-L, the PV of small pores consistently exceeds that of micropores and macropores, indicating that small pores constitute the primary component of the total PV, followed by micropores and mesopores. In contrast, CZ-A is dominated by micropores, with small pores and mesopores being secondary contributors.

(2) Pore SSA distribution characteristics

The SSA was calculated utilizing the inherent Brunauer–Emmett–Teller (BET) calculation method in the analyzer, based on the different adsorption amounts of nitrogen for the coal samples with different metamorphic degrees under various pressures, as given by:

$$\frac{P/P_0}{V(1-P/P_0)} = \frac{1}{V_m C} + \frac{C-1}{V_m C}\left(\frac{P}{P_0}\right) \quad (2)$$

where P is the adsorbate pressure, Pa; P_0 is the saturation vapor pressure of nitrogen at −196 °C, Pa; V is the actual adsorption capacity on the coal sample surface, ml; V_m is the monolayer saturation adsorption capacity of nitrogen, ml; and C is a constant related to the adsorption capacity of the experimental coal sample.

The SSAs of the coal samples were determined through liquid nitrogen adsorption experiments, and the results are presented in Table 3. According to Table 3, the total SSA of DS-L is 4.839 m^2/g, whereas that of CZ-A is 5.362 m^2/g. Notably, for both coal samples, the SSA of micropores significantly exceeds that of small pores and mesopores, with the contribution ratio of micropores exceeding 65% in both instances. This underscores the pivotal role of micropores in contributing to the overall SSA of the coal samples. Moreover, as the metamorphic degree of the coal sample rises, the SSA of micropores exhibits an upward trend.

Table 3. SSA test results of coal samples.

Coal Sample	BET SSA (m^2/g)			Total SSA (m^2/g)
	Micropores	Small Pores	Mesopores	
DS-L	3.308	1.449	0.081	4.839
CZ-A	4.712	0.519	0.130	5.362

(3) Pore shape characteristics

The DE classification method was employed to analyze the experimental coal samples [29]. The varying metamorphic degrees of the coal samples resulted in differences in their liquid nitrogen adsorption isotherms, which in turn reflected distinct pore shape characteristics, as shown in Figure 3, where type A corresponds to cylindrical holes, type B relates to fissure holes, type C and type D correspond to wedge-shaped holes, and type E relates to ink-bottle-shaped holes in porous media.

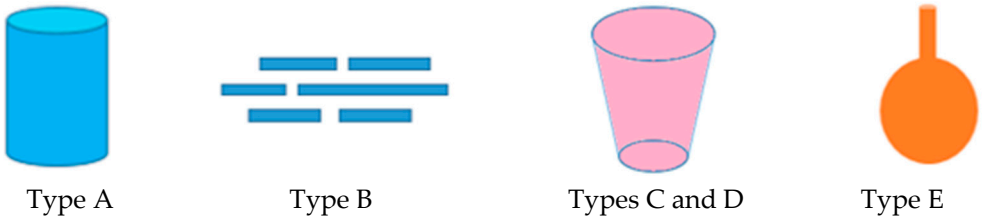
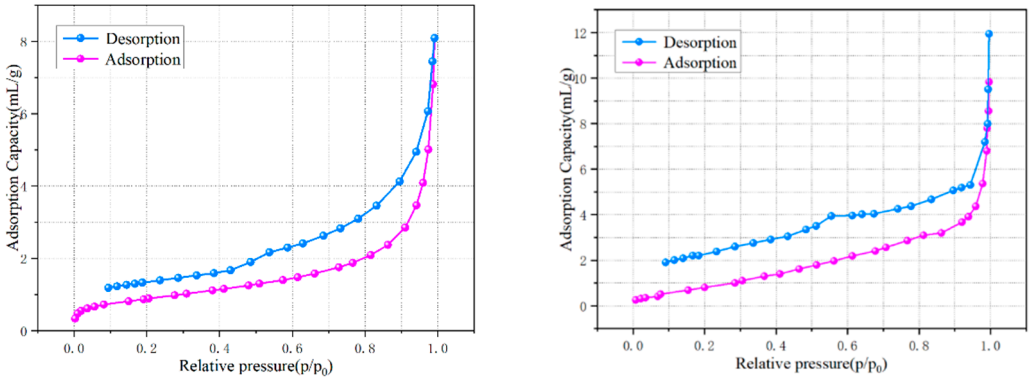


Figure 3. Pore shapes reflected by adsorption isotherms.

According to the experimental data, the liquid nitrogen adsorption isotherms for the coal samples are depicted in Figure 4.

As shown in Figure 4a, during adsorption, the liquid nitrogen adsorption and desorption isotherms of DS-L remain separated all the time, even at lower relative pressures. This observation suggests that the micropores in DS-L are well developed and dominated by cylindrical micropores with one end closed.

As shown in Figure 4b, during adsorption, the liquid nitrogen adsorption and desorption isotherms of CZ-A are also separated, with no overlap even at lower relative pressures. This finding reveals that micropores in CZ-A are also well developed and dominated by cylindrical micropores with one end closed. However, the desorption isotherm exhibits an inflection point at a relative pressure of approximately 0.5, indicative of the presence of ink-bottle-shaped micropores.



(**a**) DS-L (**b**) CZ-A

Figure 4. (**a**) Liquid nitrogen adsorption isotherms of DS-L. (**b**) Liquid nitrogen adsorption isotherms of CZ-A.

3.2. Simulation of Pore Structure Characteristics in Coal Macromolecular Models

Liquid nitrogen adsorption serves as a reliable method for the structural characterization of micropores. However, the limitations in testing methods pose challenges in acquiring the structural parameters for ultra-micropores. Consequently, this study adopts molecular simulation techniques to ascertain the pore structure parameters of ultra-micropores.

(1) SSA simulation

The SSAs of the DS-L and CZ-A macromolecular models were calculated based on the Connolly principle (Figure 5). The red area represents the surface area of the constructed molecular structure; the blue spheres represent the molecular probes used; the dashed lines depict the trajectories of the molecular probes; the arrows indicate the direction of probe movement; the gray outline represents the area enclosed by the molecular probes after completing one full circuit; and the area of the gray region corresponds to the surface area of the molecular structure.

$$Surface\ Area = \frac{Surface\ Area\ per\ cell}{Density \times Cell\ Volume} \times 10^4 \quad (3)$$

where $Surface\ Area$ denotes the Connolly SSA, m^2/g; $Surface\ Area\ per\ cell$ represents the surface area of the coal macromolecular model, $Å^2$; $Density$ stands for the density of the coal macromolecular model, g/cm^3; and $Cell\ Volume$ indicates the volume of the coal macromolecular model, $Å^3$.

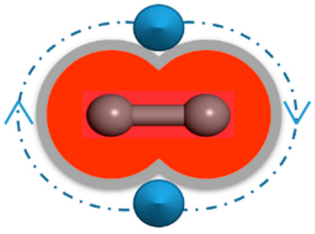
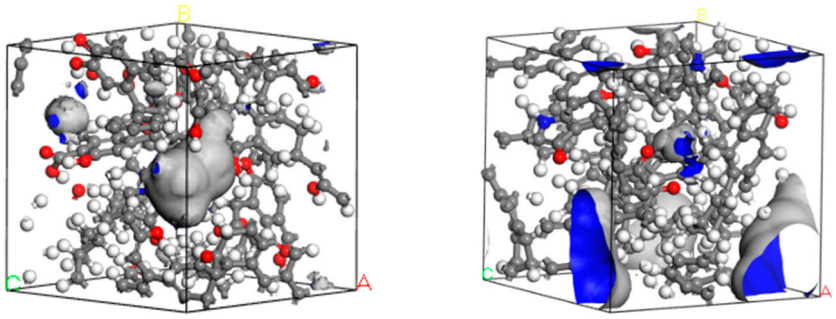


Figure 5. Diagram of the Connolly principle for the SSA calculation.

Firstly, the DS-L macromolecular model was simulated to obtain the molecular probe result under the Connolly surface (Figure 6a). By substituting the acquired result into Equation (3), the Connolly SSA of the DS-L macromolecular model was calculated to be 40.3707 m^2/g. Analogously, the Connolly SSA of the CZ-A macromolecular model was computed to be 45.5005 m^2/g, with the corresponding molecular probe result presented in Figure 6b.



(**a**) DS-L (**b**) CZ-A

Figure 6. (**a**) Molecular probe result of DS-L. (**b**) Molecular probe result of CZ-A.

(2) PV simulations

Based on the Connolly principle, the PVs of the DS-L and CZ-A macromolecular models were formulated by:

$$Pore\ Volume = \frac{Cell\ Free\ Volume}{Density \times Cell\ Volume} \quad (4)$$

where *Pore Volume* denotes the Connolly PV, cm^3/g; *Cell Free Volume* represents the free volume of the coal macromolecular model, $Å^3$; *Density* stands for the density of the coal macromolecular model, g/cm^3; and *Cell Volume* indicates the volume of the coal macromolecular model, $Å^3$.

Initially, the DS-L macromolecular model was simulated, in which the parameters were set to be identical to those employed in the prior SSA simulation. Subsequently, the obtained parameters were substituted into Equation (4) to calculate the pore PV of DS-L, yielding a value of 0.022873 cm^3/g. Analogously, the PV of the CZ-A molecular model was computed to be 0.034971 cm^3/g. The comparison of the experimental and simulation results is shown in Table 4.

Table 4. Comparison of experimental and simulation results.

Coal Sample		Total SSA (Am^2/g)	Total PV (m^3/g)
DS-L	Experiment	4.839	0.012454
	Simulation	40.3707	0.022873
CZ-A	Experiment	5.362	0.019642
	Simulation	45.5005	0.034971

For both DS-L and CZ-A, the simulated SSA and PV results are numerically larger than the corresponding experimental values. In addition, the simulated SSA and PV results of CZ-A are both greater than those of DS-L, which is consistent with the experimental findings. This discrepancy arises because the liquid nitrogen adsorption method can hardly test ultra-micropores (<2 nm) in coal. The results provided by this method only represent the SSAs of a subset of micropores, as well as mesopores and macrospores. In contrast, during molecular simulation, the SSAs of various ultra-micropores in coal can be

effectively measured by selecting molecular probes with an appropriate radius. This leads to a significant difference between the simulated and experimental results. This difference also highlights the limitations of current measurement techniques in accurately accessing ultra-micropore diameters under practical conditions.

In summary, combined with the results of liquid nitrogen adsorption experiments, it is found that micropores and ultra-micropores are extensively present in coal, and the structural characteristic parameters of the micropores and ultra-micropores of coal can be characterized by liquid nitrogen adsorption experiments and molecular simulation, and based on this, we can further carry out adsorption simulation studies on coal macromolecule models to analyze the adsorption characteristics of coal on different gases.

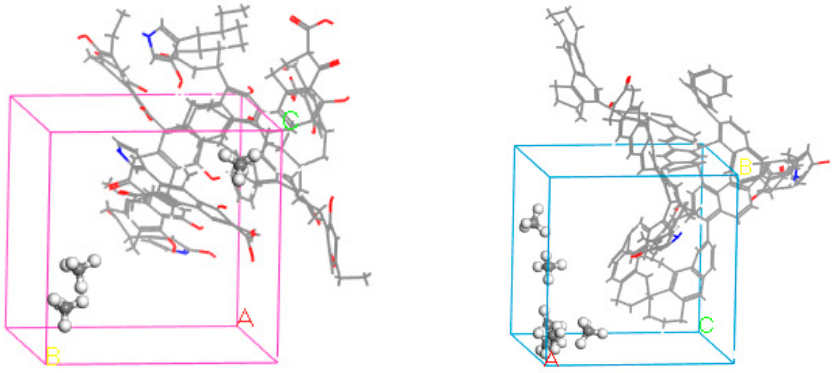
3.3. Adsorption Simulation on Coal Macromolecular Models

3.3.1. CH_4 Isothermal Adsorption Simulation

Based on the two macromolecular models of coal samples for CH_4 isothermal adsorption simulation, the number of CH_4 molecules adsorbed per unit cell at 303.15 K was obtained. The results are presented in Table 5. Additionally, the saturated adsorption configurations of macromolecules for DS-L and CZ-A after the completion of adsorption are illustrated in Figures 7a and 7b, respectively.

Table 5. CH_4 isothermal adsorption data (PCs/cell).

Pressure (MPa)	0	1	2	3	4	5	6	7	8	9	10
DS-L	0	1.76	2.85	2.98	3.09	3.18	3.25	3.31	3.35	3.38	3.4
CZ-A	0	2.28	3.98	4.36	4.67	4.89	5.08	5.19	5.28	5.35	5.37



(**a**) DS-L (**b**) CZ-A

Figure 7. (**a**) Saturated adsorption configuration of macromolecules for DS-L. (**b**) Saturated adsorption configuration of macromolecules for CZ-A.

In the isothermal adsorption simulation of macromolecular models of coal, the results are reported as the number of methane molecules per unit cell. However, in actual methane adsorption experiments, the adsorption results are typically measured in units of cm^3/g. Therefore, to compare the simulation results with experimental results, a conversion is necessary, which can be given by Equation (5):

$$1\ \text{molecular/u.c} = 1/N_A \div M \times V_{mol} \text{cm}^3/g \tag{5}$$

where N_A is Avogadro's constant, with a value of 6.02×10^{23}; M is the mass of a single unit cell, g; and V_{mol} is the molar volume of a gas at standard temperature and pressure, with a value of 22.4×10^3 cm^3.

The isothermal adsorption data converted according to Equation (5) are shown in Table 6.

Table 6. CH_4 isothermal adsorption data (cm^3/g).

Pressure (MPa)	0	1	2	3	4	5	6	7	8	9	10
DS-L	0	15.84	25.65	26.82	27.81	28.62	29.25	29.79	30.15	30.42	30.6
CZ-A	0	20.43	35.66	39.06	41.84	43.81	45.52	46.50	47.31	47.94	48.12

As can be found in Table 6, at a constant temperature, the adsorption capacities of both the DS-L and CZ-A macromolecular models exhibit a gradual increase with the rise in pressure, indicating that pressure facilitates CH_4 adsorption. Moreover, within the entire pressure gradient range, the CH_4 adsorption capacity of the CZ-A macromolecular model is always greater than that of the corresponding DS-L model.

Based on the comprehensive analysis of the experimental and simulation results related to the pore structure characteristics, CZ-A exhibits a larger SSA and PV compared to DS-L. Additionally, the CH_4 adsorption capacity of coal is positively correlated with PV, SSA, and pore size. Notably, micropores and ultra-micropores are the primary contributors to the SSA and PV of coal, suggesting that the adsorption capacity of coal for gases lies within the range of micropores to ultra-micropores. Micropores, due to their smaller diameters, offer a larger space for gas molecule adsorption, thereby enhancing gas molecule adsorption. The experimental findings by Wang et al. [30] reveal that micropore filling accounts for 74% to 99% of the total gas adsorption amount, which further emphasizes the crucial role of micropores in augmenting the gas adsorption capacity. Prior research [31,32] demonstrates that an increase in SSA and PV leads to an improvement in methane adsorption capacity, and that the adsorption capacity strengthens with the rise in the metamorphic degree.

3.3.2. CH_4 Adsorption Simulation at Different Temperatures

With the aid of Materials Studio, simulations were conducted to assess the CH_4 adsorption capacity at temperatures of 303.15 K, 313.15 K, and 323.15 K, respectively. The Sorption module within the software was utilized for these simulations, with all parameter settings maintained to be consistent with those outlined in the preceding section. According to Equation (5), the simulation outcomes were then converted to derive the CH_4 isothermal adsorption data for both the DS-L and CZ-A macromolecular models at the aforementioned temperatures (Table 7).

Table 7. CH_4 isothermal adsorption data at different temperatures (cm^3/g).

Pressure (MPa)	DS-L			CZ-A		
	303.15 K	313.15 K	323.15 K	303.15 K	313.15 K	323.15 K
0	0	0	0	0	0	0
1	15.84	14.04	12.96	20.43	18.73	17.74
2	25.65	23.94	22.95	35.66	32.70	31.81
3	26.82	25.2	24.12	39.066	36.19	34.59
4	27.81	26.28	25.2	41.84	39.25	37.45
5	28.62	27	26.01	43.81	41.57	39.07
6	29.25	27.72	26.45	45.52	43.46	40.41
7	29.79	28.35	26.9	46.50	44.53	41.66
8	30.15	28.89	27.35	47.31	45.34	42.56
9	30.42	29.25	27.62	47.94	45.88	43.28
10	30.6	29.34	27.8	48.12	45.96	43.81

Based on the data in Table 7, Langmuir fitting was performed on the CH_4 adsorption simulation results for the DS-L and CZ-A macromolecular models at different temperatures (Figures 8 and 9).

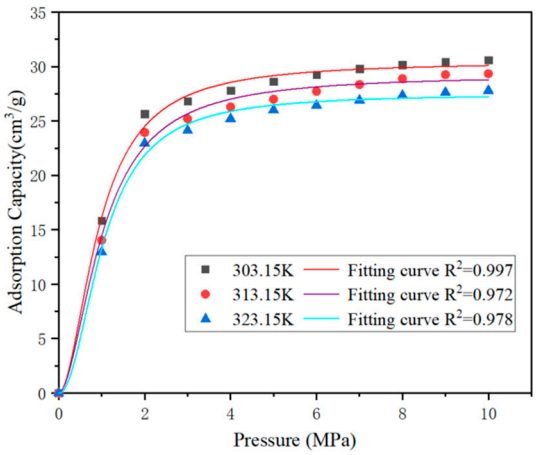


Figure 8. Isothermal adsorption curves of DS-L at different temperatures.

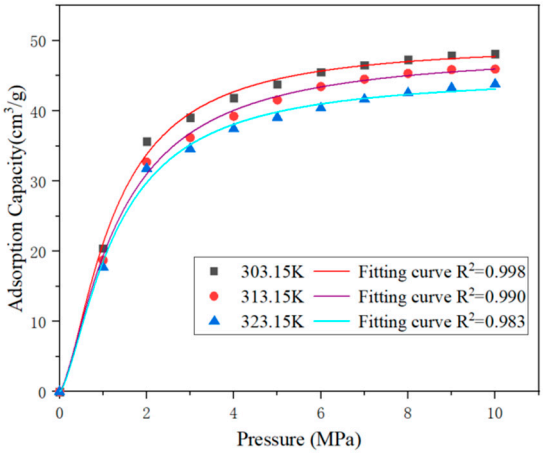


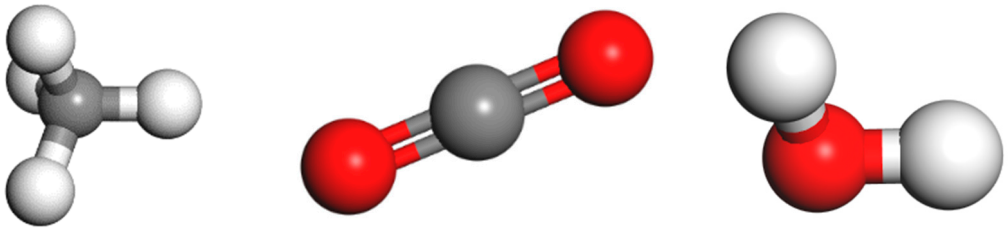
Figure 9. Isothermal adsorption curves of CZ-A at different temperatures.

Upon the analysis of Table 6 and Figures 8 and 9, it is evident that the CH_4 adsorption simulation results for both the DS-L and CZ-A macromolecular models across various temperatures adhere to the Langmuir equation. Specifically, during the initial stage of adsorption, the adsorption capacity increases rapidly with pressure. However, upon reaching a specific pressure threshold, the increase rate slows and subsequently stabilizes. Notably, with the increase in the simulation temperature, the maximum CH_4 adsorption capacity of both models has a declining trend, indicating that temperature has an inhibitory effect on CH_4 adsorption. This phenomenon is attributed to the fact that as the temperature rises, the kinetic energy of gas molecules on the coal surface is augmented, facilitating the escape of CH_4 molecules from the van der Waals forces, and consequently, reducing the CH_4 adsorption capacity. Liu and Xiao et al. [33,34] indicated that methane adsorption capacity in the coal sample decreased linearly with an increase in temperature, and the temperature effect on reducing the methane adsorption capacity was greater at low pressures. This is consistent with our research findings.

3.3.3. Isothermal Adsorption Simulation for Different Adsorbates

The analysis of the adsorption capacity of the lignite and anthracite macromolecular models for different adsorbates (CH_4, CO_2, H_2O) was conducted through adsorption simu-

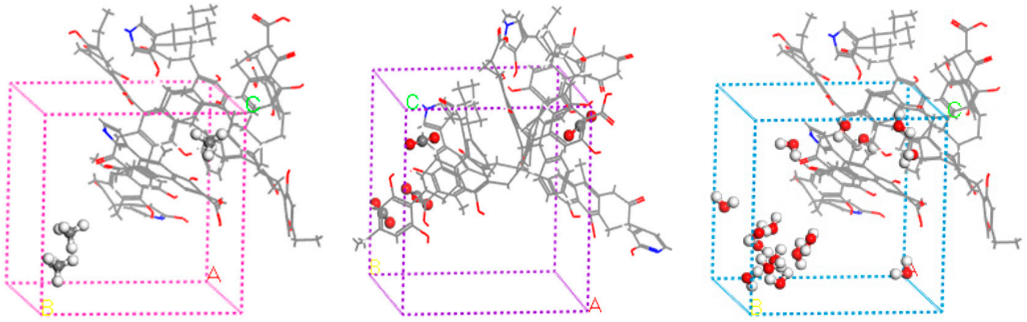
lations. Initially, the planar models of these three adsorbates were drawn in the Visualizer interface, followed by automatic hydrogen addition and clean processing for preliminary optimization. Subsequently, the Forcite module was employed to perform kinetic optimization and annealing optimization on the pre-optimized molecular models, with the optimization parameters set as described in Section 2.4. The molecular configurations of the three adsorbates after completing all optimizations are shown in Figure 10.



(**a**) CH_4 (**b**) CO_2 (**c**) H_2O

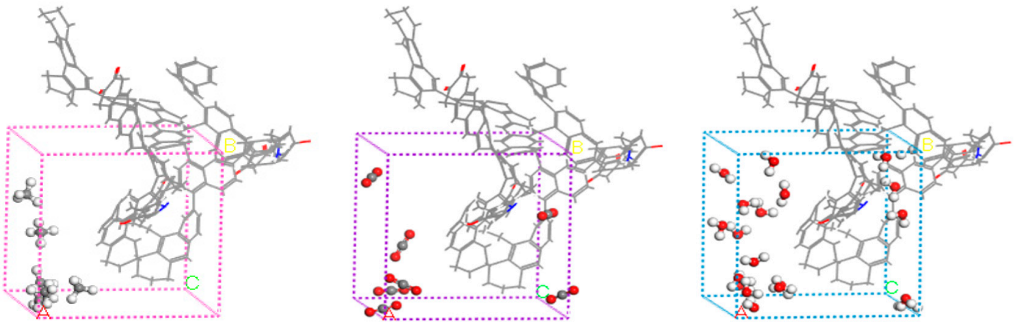
Figure 10. Molecular configurations of adsorbates.

In this simulation, the Sorption module of the software was used to investigate the adsorption behaviors of CO_2 and H_2O on the DS-L and CZ-A macromolecular models whose periodic boundary conditions had been constructed prior to the simulation. The simulation temperature was set to 303.15 K, while the other parameters were kept the same as those described in the previous section. The saturated adsorption configurations of the DS-L and CZ-A macromolecular models upon the completion of the simulation are presented in Figures 11 and 12, respectively.



(**a**) CH_4 (**b**) CO_2 (**c**) H_2O

Figure 11. (**a**) Adsorption density field of the DS-L macromolecular model after adsorbing CH_4. (**b**) Adsorption density field of the DS-L macromolecular model after adsorbing CO_2. (**c**) Adsorption density field of the DS-L macromolecular model after adsorbing H_2O.

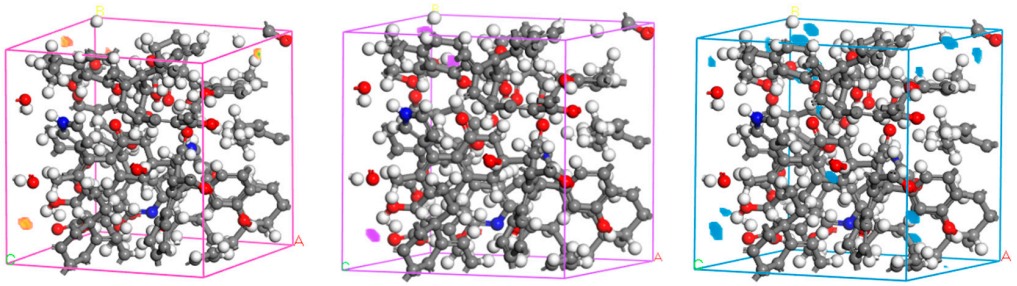


(**a**) CH_4 (**b**) CO_2 (**c**) H_2O

Figure 12. (**a**) Adsorption density field of the CZ-A macromolecular model after adsorbing CH_4. (**b**) Adsorption density field of the CZ-A macromolecular model after adsorbing CO_2. (**c**) Adsorption density field of the CZ-A macromolecular model after adsorbing H_2O.

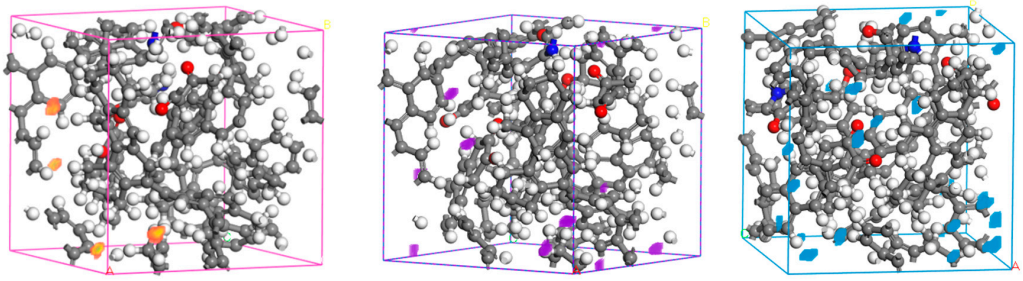
Figure 11a depicts the adsorption configuration of the DS-L macromolecular model after adsorbing three CH_4 molecules, Figure 11b shows its configuration after adsorbing four CO_2 molecules, and Figure 11c displays its configuration after adsorbing fifteen H_2O molecules. Figure 12a–c provide the adsorption configurations of the CZ-A macromolecular model after adsorbing six CH_4 molecules, seven CO_2 molecules, and nineteen H_2O molecules, respectively.

Figures 13 and 14 show the density plots of the DS-L and CZ-A macromolecular models after adsorbing CH_4, CO_2, and H_2O, respectively. The colored patches indicate the potential positions of the adsorbates, and a denser distribution of these patches is indicative of a higher adsorption capacity.



(**a**) CH_4 (**b**) CO_2 (**c**) H_2O

Figure 13. Adsorption density fields of the DS-L macromolecular model.



(**a**) CH_4 (**b**) CO_2 (**c**) H_2O

Figure 14. Adsorption density fields of the CZ-A macromolecular model.

According to the distribution of adsorbates within the CZ-A macromolecular model, it is evident that most adsorbates are adsorbed at the model boundaries. Among them, H_2O molecules exhibit the richest adsorption sites, while CH_4 molecules have the poorest. This observation can be attributed to two factors. The first factor is the Molecular Dynamic radii of the three adsorbates. Smaller radii allow for greater adsorption space within the micropores. The second factor is the properties of the adsorbates themselves. During adsorption, H_2O molecules form new adsorption sites due to capillary condensation, so they have the largest adsorption capacity. Consequently, competition for the same adsorption sites arises during multivariate adsorption processes.

Using Materials Studio, five simulations were conducted for each adsorbate under identical conditions, and their average adsorption capacities were calculated (Table 8).

Based on the data in Table 8, Langmuir fitting was performed on the simulation results obtained for the adsorption of these three different adsorbates on both the DS-L and CZ-A macromolecular models (Figure 15).

Table 8. Adsorption capacities of different adsorbates (cm^3/g).

Pressure (MPa)	DS-L CH_4	DS-L CO_2	DS-L H_2O	CZ-A CH_4	CZ-A CO_2	CZ-A H_2O
0	0	0	0	0	0	0
1	15.84	18.92	68.04	20.43	23.21	77.41
2	25.65	29.64	93.42	35.66	40.68	116.12
3	26.82	32.79	102.21	39.066	47.76	134.4
4	27.81	34.31	110.52	41.84	51.79	144.61
5	28.62	36.38	118.35	43.81	54.84	152.77
6	29.25	38.27	124.74	45.52	56.72	157.25
7	29.79	39.35	128.07	46.50	57.97	161.10
8	30.15	39.84	130.95	47.31	58.96	164.51
9	30.42	40.15	133.02	47.94	59.58	167.46
10	30.6	40.28	135	48.12	59.85	170.24

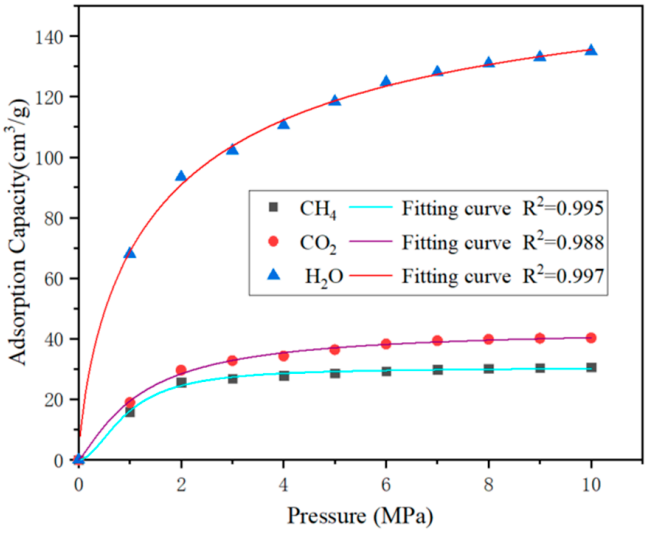


Figure 15. Isothermal adsorption curves of DS-L for different adsorbates.

As depicted in Figures 15 and 16, when the DS-L and CZ-A macromolecular models adsorb the three different adsorbates, the adsorption simulation results all conform to the Langmuir equation. Specifically, during the initial stage, the adsorption capacity increases significantly with the rise in pressure. However, the amplitude of the increase declines and tends to stabilize as the pressure reaches a certain value. Additionally, as the temperature rises, the adsorption capacity gradually declines. Under identical temperatures and pressures, the adsorption capacities of the DS-L and CZ-A macromolecular models for different adsorbates exhibit a consistent order: $H_2O > CO_2 > CH_4$. Moreover, the adsorption capacities of CZ-A surpass those of DS-L. These observations align with the research results reported by Jia [35]. That is, the competitive adsorption sequence of CO_2, CH_4, and H_2O follows the order of $H_2O > CO_2 > CH_4$. In the industrial applications of CO_2-enhanced coalbed methane recovery, the displacement efficiency often exhibits variability due to poorly understood competitive adsorption mechanisms, particularly the interference from H_2O. The simulations revealed a competitive adsorption sequence of $H_2O > CO_2 > CH_4$, indicating that priority should be given to controlling coal seam moisture to enhance CO_2 displacement efficiency. These findings can provide valuable theoretical insights for methane displacement in coal seams.

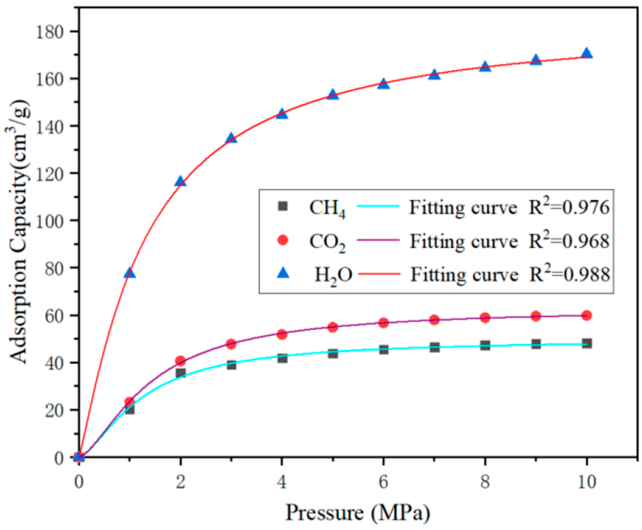


Figure 16. Isothermal adsorption curves of CZ-A for different adsorbates.

3.3.4. Energy Variations in Coal Before and After Adsorption of Different Adsorbates

To investigate the energy changes in the DS-L and CZ-A macromolecular models before and after the adsorption of CH_4, CO_2, and H_2O, isothermal adsorption simulations were conducted, and the energy change data were extracted accordingly. Tables 9 and 10 give the energy variations in the DS-L and CZ-A macromolecular models before and after the saturation adsorption of these three adsorbates, respectively.

Table 9. Energy changes in DS-L before and after adsorption of different adsorbates.

	Total Energy (Kcal/mol)	Valence Electron Energy (Kcal/mol)				Non-Bond Interaction Energy (Kcal/mol)		
		Bond	Angle	Torsion	Inversion	van der Waals	Electrostatic	H-Bond
Before adsorption	474.014	83.528	132.248	146.933	5.908	277.366	−152.935	−1.082
After CH_4 adsorption	443.325	83.527	132.136	146.932	5.907	241.572	−163.057	−1.094
After CO_2 adsorption	432.986	83.527	133.056	146.933	5.906	235.158	−172.356	−2.321
After H_2O adsorption	385.784	83.342	132.247	146.931	5.907	283.237	−246.236	−32.756

Table 10. Energy changes in CZ-A before and after adsorption of different adsorbates.

	Total Energy (Kcal/mol)	Valence Electron Energy (Kcal/mol)				Non-Bond Interaction Energy (Kcal/mol)		
		Bond	Angle	Torsion	Inversion	van der Waals	Electrostatic	H-Bond
Before adsorption	3595.511	1973.913	124.974	125.717	5.436	1233.536	−185.102	−3.327
After CH_4 adsorption	3157.256	1900.921	114.130	114.620	4.392	852.129	−225.942	−3.432
After CO_2 adsorption	2546.362	1836.315	120.074	113.646	5.931	901.308	−426.909	−5.366
After H_2O adsorption	1532.596	1364.367	132.368	120.575	6.354	1122.354	−1412.704	−235.653

As can be seen in Table 9, for DS-L, the total energy changes are 30.689 Kcal/mol, 41.028 Kcal/mol, and 88.23 Kcal/mol upon adsorbing the three adsorbates. The magnitude of the decrease follows the order of H_2O > CO_2 > CH_4. In terms of valence electron energy, minimal changes are observed; less than 1% on average. Regarding non-bond interaction energy, van der Waals energy changes more noticeably than electrostatic energy and hydrogen bonding energy for CH_4 and CO_2 adsorption, while electrostatic energy and hydrogen bonding energy change more significantly than van der Waals energy for H_2O adsorption. This suggests that CH_4 and CO_2 primarily adsorb on the models through the van der Waals forces, whereas H_2O predominantly adsorbs on the models through

electrostatic and hydrogen bonding forces. Consequently, physical adsorption dominates in the adsorption of CH_4 and CO_2 by DS-L, whereas physical and chemical adsorption coexist in the adsorption of H_2O. As demonstrated in the study by Kang et al. [36], CO_2 exhibits not only physical adsorption but also chemical adsorption, while H_2O only demonstrates physical adsorption. Similarly for CZ-A, Table 10 reveals that physical adsorption is predominant in the adsorption of CH_4 and CO_2, and physical and chemical adsorption occur simultaneously in the adsorption of H_2O.

4. Conclusions

(1) The PV of DS-L predominantly comprises small pores, whereas the PV of CZ-A is chiefly characterized by micropores. The SSA of micropores constitutes more than 65% of the total SSA in both coal samples, suggesting that micropores are the primary contributors to the SSA of adsorption pores. Utilizing the constructed macromolecular models, the SSAs and PVs of the DS-L and CZ-A coal samples are simulated by employing N_2 molecule probes. The SSAs and PVs of the obtained coal samples are 40.3707 m^2/g and 45.5005 m^2/g, and 0.022873 cm^3/g and 0.034971 cm^3/g, respectively. The simulation outcomes for both coal samples exceed the experimental results, which demonstrates that molecular simulations represent an effective means of measuring pore structure parameters across various ultra-micropores in coal.

(2) The CH_4 adsorption amount of the CZ-A macromolecular model consistently surpasses that of the corresponding DS-L macromolecular model. Moreover, the CH_4 adsorption amount exhibits a positive correlation with the SSA and PV of coal.

(3) The maximum CH_4 adsorption amounts of both the DS-L and CZ-A macromolecular models diminish as the temperature increases, indicating a suppressive effect of temperature on CH_4 adsorption. When the two models adsorb CH_4, CO_2, and H_2O, the adsorption amounts follow the order of $H_2O > CO_2 > CH_4$. Analysis of the energy changes before and after adsorption reveals that the adsorption of CH_4 and CO_2 by DS-L and CZ-A is predominantly physical, whereas that of H_2O encompasses both physical and chemical adsorption.

Author Contributions: P.C.: Conceptualization, Funding acquisition, Methodology, Investigation, Writing—original draft, Writing—review and editing. Y.W.: Conceptualization, Methodology, Formal analysis, Investigation, Writing—original draft. Y.Z.: Methodology, Formal analysis, Investigation, Writing—review and editing. Q.W.: Investigation, Writing—original draft. Z.W.: Investigation, Writing—original draft. L.T.: Investigation, Writing—original draft. All authors have read and agreed to the published version of the manuscript.

Funding: This work was supported by the Program for National Natural Science Foundation of China (52274191), and the project was funded by China Postdoctoral Science Foundation (2021M700132) and the Basic Research Funds of Henan Polytechnic University (NSFRF220205).

Data Availability Statement: The raw data supporting the conclusions of this article will be made available by the authors on request.

Conflicts of Interest: Author Pan Chen was employed by the company JiaoZuo Coal Industry (Group) Co., Ltd.. The remaining authors declare that the research was conducted in the absence of any commercial or financial relationships that could be construed as a potential conflict of interest.

Nomenclature

r_k	Pore radius of the experimental coal sample	nm
σ_1	Surface tension of the condensed phase	N/m
V	Actual adsorption capacity on the coal sample surface	mL
V_m	Monolayer saturation adsorption capacity of nitrogen	mL

V_{m1}	Adsorption volume of the liquid under the action of liquid nitrogen	cm^3/g
R	Gas constant	$J \cdot mol^{-1} \cdot K^{-1}$
T_b	Experimental temperature	K
P	Pressure of the adsorbate	Pa
P_0	Saturation vapor pressure of nitrogen at −196 °C	Pa
Surface Area	Connolly SSA	m^2/g
Surface Area per cell	Surface area of the coal macromolecular model	$Å^2$
Density	Density of the coal macromolecular model	g/cm^3
Cell Volume	Volume of the coal macromolecular model	$Å^3$
Pore Volume	Connolly PV	cm^3/g
Cell Free Volume	Free volume of the coal macromolecular model	$Å^3$
Density	Density of the coal macromolecular model	g/cm^3
Cell Volume	Volume of the coal macromolecular model	$Å^3$
M	Mass of a single unit cell	g
V_{mol}	Molar volume of a gas at a standard temperature and pressure	cm^3

References

1. Ge, S.; Fan, J.; Liu, S.; Song, M.; Xian, Y.; Wang, B.; Teng, T. Low carbon modern coal-based energy technology system and development strategy. *J. China Coal Soc.* **2024**, *49*, 203–223.
2. Zhang, D.; Zhu, J.; Zhao, X.; Gao, Y.; Geng, M.; Chen, G.; Jiao, J.; Liu, S. Dynamic assessment of coalbed methane resources and availability in China. *J. China Coal Soc.* **2018**, *43*, 1598–1604.
3. Xu, F.; Hou, W.; Xiong, X.; Xu, B.; Wu, P.; Wang, H.; Feng, K.; Yun, J.; Li, S.; Zhang, L.; et al. The status and development strategy of coalbed methane industry in China. *Petroleum Explor. Dev.* **2023**, *50*, 765–783. [CrossRef]
4. Cheng, Y.; Hu, B. Main occurrence form of methane in coal: Micropore filling. *J. China Coal Soc.* **2021**, *46*, 2933–2948.
5. Zhou, J.; Guo, X.; Zhao, B.; Jin, Z.; Deng, C. Study on the influence of microscopic components and pore structure of coal-rock system on methane adsorption. *Min. Saf. Environ. Prot.* **2024**, *51*, 51–60.
6. Yi, M.; Cheng, Y.; Wang, Z.; Wang, C.; Hu, B.; He, X. Effect of particle size and adsorption equilibrium time on pore structure characterization in low pressure N_2 adsorption of coal: An experimental study. *Adv. Powder Technol.* **2020**, *31*, 4275–4281. [CrossRef]
7. Liu, H.; Mou, J.; Cheng, Y. Impact of pore structure on gas adsorption and diffusion dynamics for long-flame coal. *J. Nat. Gas Sci. Eng.* **2015**, *22*, 203–213. [CrossRef]
8. Zhang, C.; Jia, S.; Huang, X.; Shi, X.; Zhang, T.; Zhang, L.; Wang, F. Accurate characterization method of pores and various minerals in coal based on CT scanning. *Fuel* **2024**, *358*, 130128. [CrossRef]
9. Zhao, P.; He, B.; Zhang, B.; Liu, J. Porosity of gas shale: Is the NMR-based measurement reliable. *Pet. Sci.* **2022**, *19*, 509–517. [CrossRef]
10. Han, W.; Zhou, G.; Gao, D.; Zhang, Z.; Wei, Z.; Wang, H.; Yang, H. Experimental analysis of the pore structure and fractal characteristics of different metamorphic coal based on mercury intrusion-nitrogen adsorption porosimetry. *Powder Technol.* **2020**, *362*, 386–398. [CrossRef]
11. Dantas, S.; Struckhoff, K.C.; Thommes, M.; Neimark, A.V. Pore size characterization of micro-mesoporous carbons using CO_2 adsorption. *Carbon* **2021**, *173*, 842–848. [CrossRef]
12. Wen, H.; Liu, M.; Fan, S.; Wei, G.; Liu, Y.; Hao, J. Experimental study on variations of pore-fissure in coal-rock leached by liquid CO_2. *J. Xi'an Univ. Sci. Technol.* **2020**, *40*, 935–944.
13. Luo, M.; Glover, P.W.J.; Zhao, P.; Li, D. 3D digital rock modeling of the fractal properties of pore structures. *Mar. Pet. Geol.* **2020**, *122*, 104706. [CrossRef]
14. Xu, Z.; Lin, M.; Jiang, W.; Xu, L.; Ji, L.; Cao, G.; Hao, W. Pore-morphology-based pore structure characterization for various porous media. *Chem. Eng. Sci.* **2023**, *280*, 118982. [CrossRef]
15. Liu, S.; Sun, H.; Zhang, D.; Yang, K.; Li, X.; Wang, D.; Li, Y. Experimental study of effect of liquid nitrogen cold soaking on coal pore structure and fractal characteristics. *Energy* **2023**, *275*, 127470. [CrossRef]
16. Li, Y.; Zhang, Y.; Zhang, L.; Hou, J. Characterization on pore structure of tectonic coals based on the method of mercury intrusion, carbon dioxide adsorption and nitrogen adsorption. *J. China Coal Soc.* **2019**, *44*, 1188–1196.
17. Ren, P.; Xu, H.; Tang, D.; Li, Y.; Chen, Z.; Sun, C.; Zhang, F.; Chen, S.; Xin, F.; Cao, L. Pore structure and fractal characterization of main coal-bearing synclines in western Guizhou, China. *J. Nat. Gas Sci. Eng.* **2019**, *63*, 58–69. [CrossRef]

18. Li, S.; Zhou, Y.; Hu, B.; Qin, X.; Kong, X.; Bai, Y.; Zhang, J. Structural characteristics of adsorption pores in low-rank coals and their effects on methane adsorption performance. *Coal Geol. Explor.* **2023**, *51*, 127–136.
19. Zhang, S.; Tang, S.; Li, Z.; Liu, B.; Wang, R. Effect of pore structure on competitive sorption and diffusion of mixed methane and carbon dioxide in anthracite, South Qinshui Basin, China. *Int. J. Coal Geol.* **2022**, *253*, 103956. [CrossRef]
20. Dong, K.; Zhai, Z.; Guo, A. Effects of pore parameters and functional groups in coal on CO_2/CH_4 adsorption. *ACS Omega* **2021**, *48*, 32395–32407. [CrossRef]
21. Ren, X.; Wen, Z.; Song, H.; Liang, S. Experimental study on change of coal adsorption characteristics by using Fenton reagent. *Coal Technol.* **2016**, *35*, 173–175.
22. Han, Q.; Deng, C.; Jin, Z.; Gao, T. Molecular Simulation of the Adsorption Characteristics of Methane in Pores of Coal with Different Metamorphic Degrees. *Molecules* **2021**, *26*, 7217. [CrossRef]
23. Wang, Y.; Zhu, Y.; Liu, S.; Zhang, R. Pore characterization and its impact on methane adsorption capacity for organic-rich marine shales. *Fuel* **2016**, *181*, 227. [CrossRef]
24. Jiang, J.; Cheng, Y.; Zhang, S. Quantitative characterization of pore structure and gas adsorption and diffusion properties of low-rank coal. *J. China Coal Soc.* **2021**, *46*, 3221–3233.
25. Wang, Y. Characteristics of nano-pore structure of Dongqu No.2 coal and its interaction with $CH_4/CO_2/H_2O/N_2$. Master's Thesis, Taiyuan University of Technology, Taiyuan, China, 2022.
26. Wang, H.; Xiang, J.; Deng, X. Molecular Simulation of the Pore Structure and Adsorption Properties of Coal under Compression Stress. *Energy Fuels* **2023**, *37*, 1887–1895. [CrossRef]
27. Yan, J.; Jia, B.; Liu, B.; Zhang, J. Simulation Study on Molecular Adsorption of Coal in Chicheng Coal Mine. *Molecules* **2023**, *28*, 3302. [CrossRef]
28. Wen, Z.; Wang, Y.; Wei, J.; Wang, J.; Si, L.; Wang, Q. Study on Molecular Model Construction and Gas Adsorption Simulation of Anthracite in the Qinshui Basin. *Langmuir* **2023**, *39*, 12944–12955. [CrossRef]
29. Liu, X. Study on Microstructural Characteristics of Coal Surface and the Mechanism of Electromagnetic Radiation. Ph.D. Thesis, China University of Mining & Technology, Beijing, China, 2019.
30. Wang, Z.; Hao, C.; Wang, X.; Wang, G.; Ni, G.; Cheng, Y. Effects of micro-mesopore structure characteristics on methane adsorption capacity of medium rank coal. *Fuel* **2023**, *351*, 128910. [CrossRef]
31. Xiao, P.; Du, Y. Experiment on the influence of microstructure of tectonic coal on its adsorption characteristics. *J. Xi'an Univ. Sci. Technol.* **2021**, *41*, 237–245.
32. Xin, F.; Xu, H.; Tang, D.; Liu, D.; Cao, C. Problems in pore property testing of lignite: Analysis and correction. *Int. J. Coal Geol.* **2021**, *245*, 103829. [CrossRef]
33. Liu, Y.; Zhu, Y.; Liu, S.; Li, W.; Tang, X. Temperature effect on gas adsorption capacity in different sized pores of coal: Experiment and numerical modeling. *J. Pet. Sci. Eng.* **2018**, *165*, 821–830. [CrossRef]
34. Xiao, T.; Li, S.; Long, H.; Kong, X.; Bai, Y.; Qin, A. Experimental research on adsorption characteristics of N_2, CH_4, and CO_2 in coal under different temperatures and gas pressures. *Energy Sci. Eng.* **2023**, *11*, 637–653. [CrossRef]
35. Jia, J.; Xing, Y.; Li, B.; Jia, P.; Wu, Y.; Yang, Q.; Wang, D. Molecular simulations of multivariate competitive adsorption of CH_4, CO_2 and H_2O in gas-fat coal. *Colloids Surf. A* **2024**, *683*, 132917. [CrossRef]
36. Kang, G.; Zhang, B.; Kang, T.; Guo, J.; Zhao, G. Effect of Pressure and Temperature on CO_2/CH_4 Competitive Adsorption on Kaolinite by Monte Carlo Simulations. *Materials* **2020**, *13*, 2851. [CrossRef]

Disclaimer/Publisher's Note: The statements, opinions and data contained in all publications are solely those of the individual author(s) and contributor(s) and not of MDPI and/or the editor(s). MDPI and/or the editor(s) disclaim responsibility for any injury to people or property resulting from any ideas, methods, instructions or products referred to in the content.